J. Mater. Environ. Sci. 8 (1) (2017) 160-168
ISSN : 2028-2508
CODEN: JMESCN

Sol-gel Aluminum-doped ZnO thin films: synthesis and characterization

T. Jannane[a], M. Manoua [a], A. Liba[*a], N. Fazouan [a], A. El Hichou [b], A. Almaggoussi [b], A. Outzourhit [c], M. Chaik [c]

(a) Laboratory of material physics, Sultan Moulay Sliman University, Sciences and technologies Faculty, BP 523, 23000 *Beni Mellal, Morocco.*
(b) Study Group of Optoelectronic Materials, Cadi Ayyad University, Sciences and technologies Faculty, BP 549, 40000 Marrakech, Morocco.
(c) Laboratory of solid physics and thin films, Cadi Ayyad University, Faculty of Sciences Semlalia, BP 549, 40000 Marrekech, Morocco.

Received 02 Aug 2016, Revised 10 Nov 2016, Accepted 13 Nov 2016
**For correspondence: Email: liba03@yahoo.fr (A. Liba); Phone: +212 662135507*

Abstract
Zinc oxide is one of the most important n-type semi-conductor intensively utilized in solar cells, transparent conducting electrodes and opto-electronic devices. Zinc oxide (ZnO) and Aluminum- doped Zinc oxide (AZO) thin films have been deposited by the spin-coating method. Their structural, optical and electrical proprieties were investigated. The X-Ray diffraction shows the polycrystalline hexagonal wurtzite structure exhibiting degradation in crystallinity of elaborated films with increasing Al doping concentration. This effect is reflected on optical and electrical proprieties of films. Indeed, the samples present a low optical transmittance level and the band gap values between 3.17 eV and 3.20 eV. Concerning the electrical properties, a decrease in the concentration of free charges carriers is observed as well as a decrease in resistivity.

Keywords: ZnO, Sol gel, Spin coating, Structural properties, Optical properties, Electrical properties.

1. Introduction
Zinc oxide thin films have attracted more attention due to their broad range of applications such as transparent electrodes in solar cells and flat panel displays, view their dual properties, a good electrical conductivity and high optical transparency in the visible range [1, 2, 3]. ZnO is a direct wide band gap (3,37 eV) semiconductor with high excitonic binding energy (60 meV) at room temperature [4, 5, 6]. Undoped and doped ZnO films have been deposited by different methods such us sputtering [7], CVD deposition [8], electro-deposition process [9], spray pyrolysis [10, 11, 12] and sol gel deposition [13, 14, 15]. The sol gel technique is one of attractive method because it allows to easily obtaining good thin films at low cost. In this work we have deposited the Al-doped ZnO thin films on glass substrate at different Al content (of 1% to 5%) by spin-coating method. Our aim is to study the effect of aluminum concentration on the structural, optical and electrical properties.

2. Experimental
The thin films were deposited by spin-coating technique on the glass substrate. Zinc acetate dehydrate ($Zn(CH_3COO)_2,2H_2O$) was used as precursor, ethanol and monoethanolamine (MEA) were used as a solvent and stabilizer respectively. Zinc acetate was firstly dissolved in ethanol, then the stabilizer was added to obtain a

transparent and homogeneous solution. The molar ratio of MEA to zinc acetate was maintained at 1.0 and the concentration of zinc acetate was 0.5 M. For Al:ZnO we are used the aluminum nitrate hexahydrate ($Al(NO_3)_2,6H_2O$) in molar ratio [Al/Zn] varying between 1 to 5%.

To elaborate our thin films, we've used the spin coater model (LAURELL WS-650MZ 23NPP /OND / UD3 /UD3B) equipped with three injection syringes. The all system is controlled by software called Spin 3000.

All films were elaborated at 48 hours sol aging time. The glass substrates were rotated at 2000 rpm for 10s after be cleaned in ethanol, acetone and rinsed in distilled water, and subsequently dried. The films were preheated at 100 °C for 5 min, then at 300 °C for 5 min to evaporate the solvent and remove organic residuals. The procedure from coating to preheating was repeated 10 times. Then the films were annealed at 500 °C for 2 hours. Figure 1 shows a schematic of the deposition process.

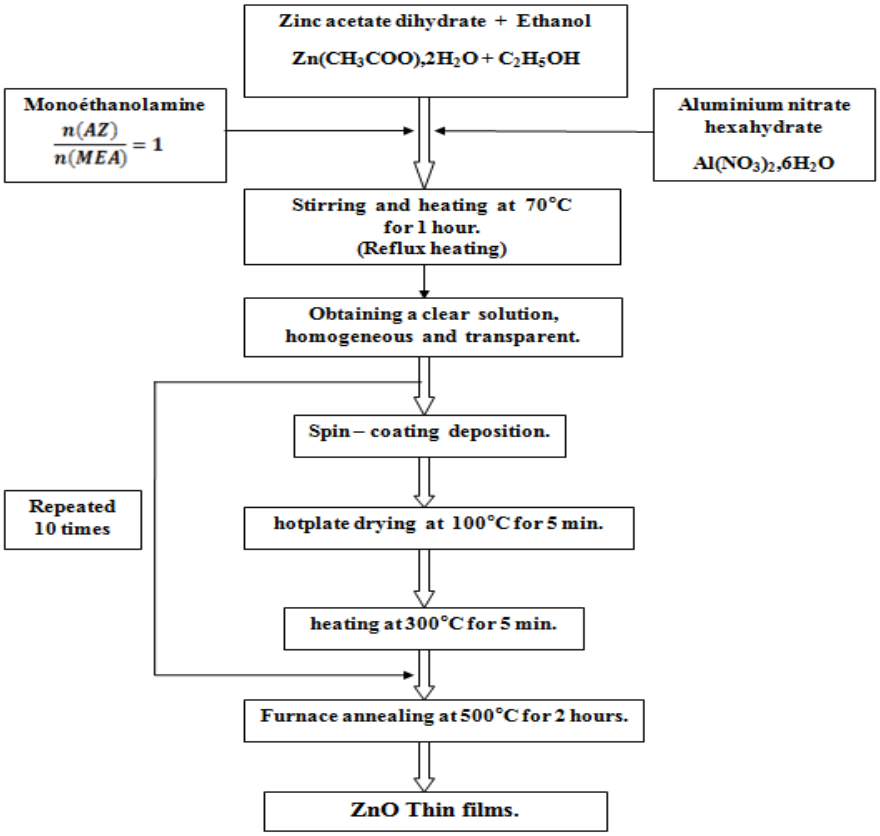

Figure 1: Process flow chart showing the procedure of thin films deposition.

The crystalline structure was analyzed by X-ray diffractometer (Philips X'Pert MPD). The optical properties were obtained by UV–Vis-NIR double beam spectrophotometer (UV- 3101PC-SHIMADZU). The electrical measurements were measured by a four-point probe method and Hall Effect (HMS5000 system).

3. Results and discussion

3.1. *Structural properties of the ZnO thin films*

The XRD spectra of films at different Aluminum doping concentration (from 1% to 5%) are shown in Figure 2. It indicated that the three pronounced peaks (100), (002) and (101) characterize a polycrystalline ZnO hexagonal wurtzite structure [15]. The first remark is the enhancement in crystallinity of films for 1% Al-doped ZnO thin films, with a preferential orientation along (002) direction, Moreover, beyond the 1%, the peak intensities decreased with increasing doping concentrations which indicates a deterioration in the crystallinity of films, with

not preferred growth orientation. This suggests that Al atoms in the ZnO structure may restrict the grain growth of ZnO films due to the lowest ionic radius of Al^{3+} than Zn^{2+} as observed in others reports like M. Yilmaz et al [16], S. Ilican et al [17], Chien-Yie Tsay et al [18] and Z.Q. Xu, H. Deng [19].

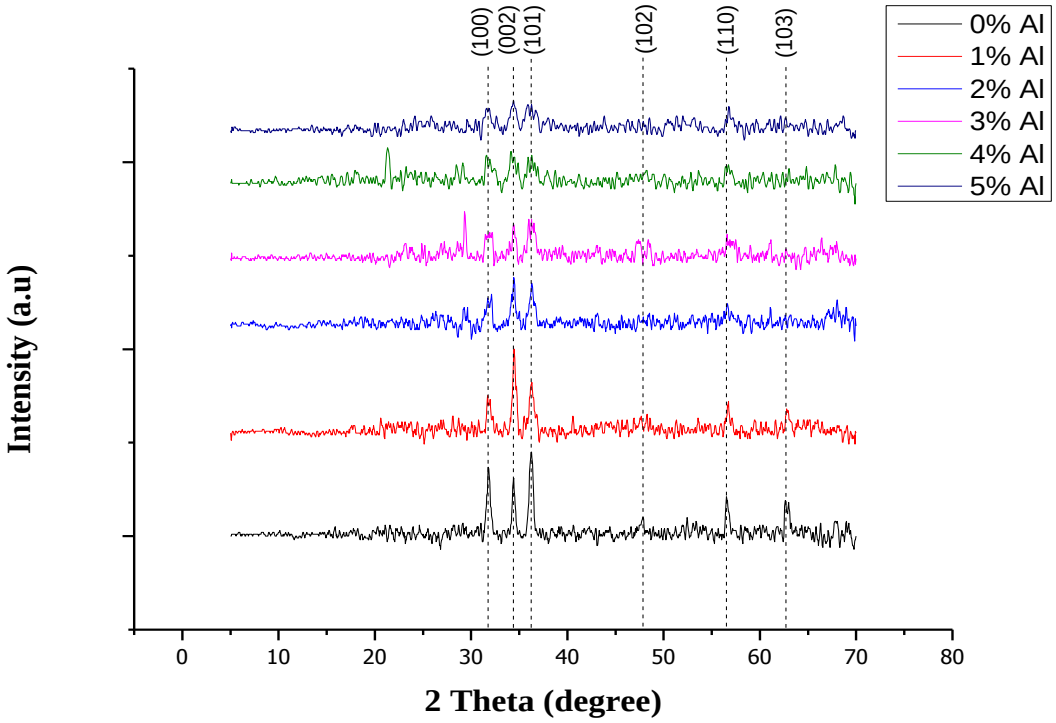

Figure 2: The XRD pattern of the undoped and doped ZnO thin films at different Al concentration.

The lattice constants can be calculated by using the following formula:

$$\frac{1}{d_{hkl}^2} = \frac{4}{3}\left[\frac{h^2 + hk + k^2}{a^2}\right] + \frac{l^2}{c^2}$$

Where **a** and **c** are the lattice constants and $\mathbf{d_{hkl}}$ is the crystalline plane distance for indices (hkl).

$$a = \frac{\lambda}{\sqrt{3}\,.\,\sin\theta_{hkl}} \qquad\qquad c = \frac{\lambda}{\sin\theta_{hkl}}$$

The lattice parameters **a** and **c** are listed in the Table 1, and distinctly show that for 1% the **c** parameter decrease while the **a** parameter increase, meaning the good insertion of Al atoms in the substitutionnal Zn sites, seen the difference of electronegativity between Aluminum and Zinc ions [20]. When the dopant concentration increase, the lattice parameters **a** and **c** increase. This effect can be due to incorporation of Al atoms in the interstitial positions of host lattice [21].

The crystallite size **D** and the strain **Ɛ** were calculated by using the Williamson's and Hall's formula as indicated below [22]:

$$\beta_{hkl} = \frac{0{,}9 * \lambda}{D\,.\cos\theta_{hkl}} + 4.\varepsilon.\tan\theta_{hkl}$$

$$\beta_{hkl}\,.\cos\theta_{hkl} = \frac{0{,}9 * \lambda}{D} + 4.\varepsilon.\sin\theta_{hkl}$$

Where β_{hkl} is the full width at half- maximum of the XRD peak, λ is the X-ray wavelength, θ_{hkl} is the Bragg diffraction angle and **Ɛ** is the strain. By tracing ($\beta_{hkl}.\cos\theta_{hkl}$) versus ($4.\sin\theta_{hkl}$), we can determine the slope which defines the strain **Ɛ**, and the crystallite size **D** can be calculated by using an extrapolation of the linear portion of [$\beta_{hkl}.\cos\theta_{hkl} = f(4.\sin\theta_{hkl})$] as shown in Figure 3.

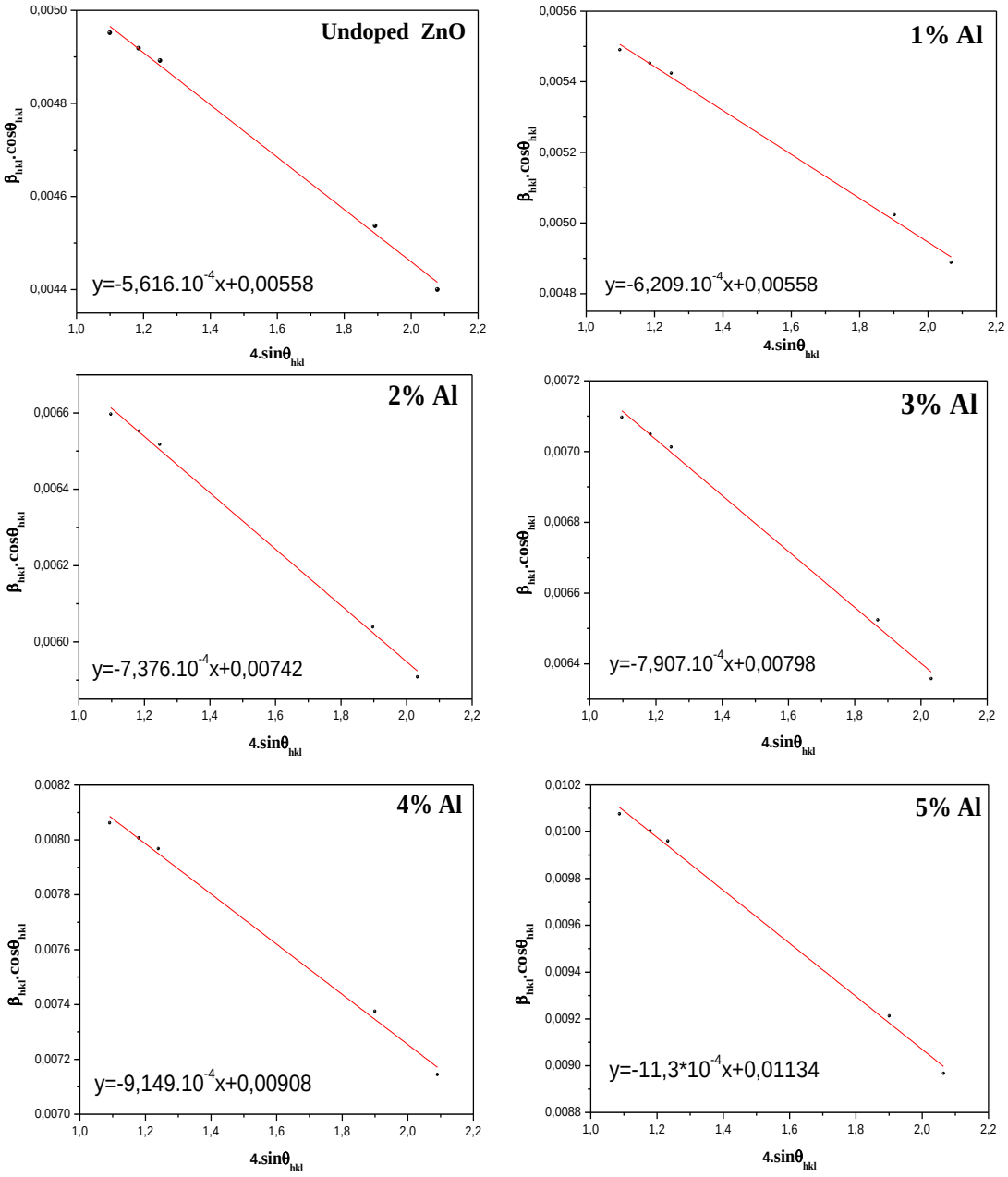

Figure 3: The W-H analysis for undoped and doped ZnO thin films at different Al concentrations.

The calculated results are listed in Table 1.

As shown in Table 1, when the Al dopant concentration increase from 0% to 5%, the crystallite size decrease from 248 to 122 Å, this result is agree with the crystalline degradation observed in the DRX spectra, this may be due to an increase in size of grain boundaries as is suggested above. Mehmet et al [16] and Shankar et al [23] have also faced with the same situation.

Other components affecting the crystal growth include the formation of strain in the lattice due to the incorporation of dopant. The positive and negative strain values represent the tensile strain when the film is stretched and the compressive strain when the film is compressed, respectively.

As illustrated in Table 1, all the values of the strain are negative, which means that there are compressive stresses in the films due to a small aluminum ionic radius than zinc ionic radius. The strains increase while increasing the Aluminum doping level [19].

Table 1: Structural parameters of pure ZnO and AZO films.

% [Al]	FWHM β (rad)	D (Å)	a (Å)	c (Å)	ε
0%	0.00515	248.484	3.2366	5.1971	-5.616×10^{-4}
1%	0.00571	223.997	3.2396	5.1953	-6.209×10^{-4}
2%	0.06860	186.865	3.2416	5.2040	-7.376×10^{-4}
3%	0.00733	173.752	3.2428	5.2082	-7.908×10^{-4}
4%	0.00838	152.703	3.2616	5.2248	-9.149×10^{-4}
5%	0.01047	122.270	3.2748	5.2248	-11.3×10^{-4}

3.2. *Optical properties of the ZnO thin films*

The effect of Al doping on optical properties of ZnO films has been studied. The transmission spectra of Al-doped ZnO films in the range of 300-2000 nm with various doping concentrations are plotted in Figure 4.

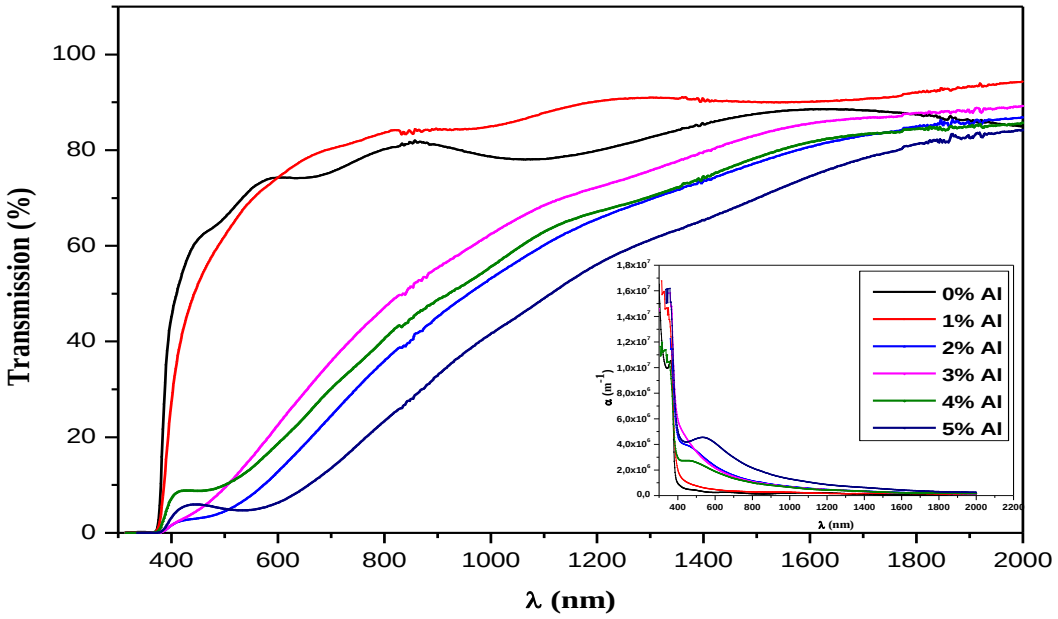

Figure 4: Variation of transmission and absorption coefficient versus the wavelength for undoped and doped ZnO thin films.

The evolution of the transmission T (λ) seen in Figure 4 shows that the 1% Al-doped ZnO thin films exhibit a good optical transmission in the visible range which can reach 85% compared to undoped ZnO. As long as, the dopant concentration increased from 2% to 5%, the optical transmission decreases [24]. This result is in good agreement with the crystalline degradation observed in the structural properties. Insight Figure 4 we represent the coefficient absorption α which is calculated using the formula below:

$$\alpha = \frac{1}{e} \ln\left(\frac{1}{T}\right)$$

Where T is the transmittance and e is the thickness of the thin films.
All the films have a strong absorption region corresponding to the wavelengths lower than 400 nm, this absorption declines subsequently in the visible range.

To estimate the optical band-gap energy, we have used the Tauc's equation [25]:
$(\alpha h\vartheta)^2 = \beta(h\vartheta - E_g)$

Where β is an energy-independent constant, hυ is the photon energy, E_g is the optical band gap and α is the absorption coefficient. The optical band gap E_g was estimated by using an extrapolation of the linear portion of $(\alpha h\nu)^2$ versus hν as shown in Figure 5.
The fact that all films had a similar thickness enabled the direct comparison of obtained optical band gap. As shown insight Figure 5, the optical band gap E_g value increased to a maximum (3.206eV) with increasing Al concentrations. The increase of the E_g with increasing the Al-concentration is may be attributed to the Moss–Burstein effect [26, 27]. The electrons may occupy the doping level which is relatively higher than the lowest level of the conduction band. Mridra and Basak [28] also reported that the optical band gap values of sol-gel spin coated ZnO thin films increased from 3.33 eV to 3.70 eV with Al doping concentration.

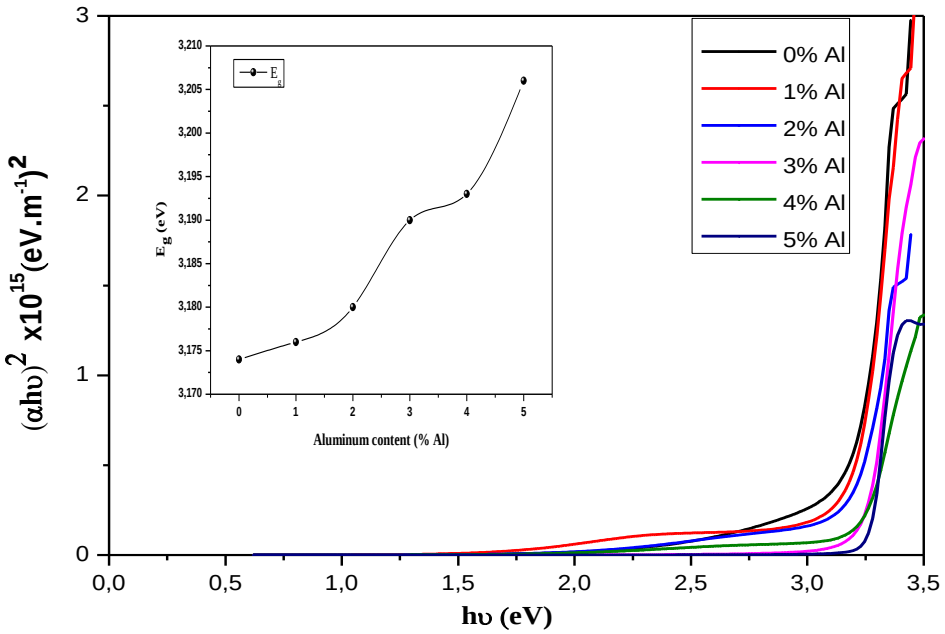

Figure 5: $(\alpha h\nu)^2$ versus hν and variation of the optical band gap as a function of aluminum concentration.

The Urbach energy E_u represents the states located at the tail of the valence and conduction bands and can be determined by the following relation [29]:

$$\alpha = \alpha_0 . \exp\left(\frac{h\square}{E_u}\right)$$

Where α_0 is the pre–exponential factor.

The Urbach energy E_u is obtained from the inverse of the slope acquired by fitting the linear part of lnα versus hυ. In Table 2, we listed the values of E_g, E_u and 1/D representing the disorder in the films where D is the crystallite size.

Table 2: Values of E_g, E_u and 1/D for different Aluminum dopant concentrations.

% Al	E_g (eV)	E_u (eV)	1/D ($Å^{-1}$)
0	3.174	0.1399	0.00402
1	3.176	0.1790	0.00446
2	3.180	0.2360	0.00535
3	3.190	0.2510	0.00576
4	3.193	0.2590	0.00655
5	3.206	0.2610	0.00818

As observed in Table 2, we obtained an increment of Urbach energy with the dopant concentration, and in the same time an increase of the disorder in the films. This disorder, is in perfect agreement with the structural degradation already observed, and creates localized states in the bandgap inducing an increase in the Urbach energy. This result was already found by B. N. Pawar [30] and F. Chouikh [24].

3.3. *Electrical properties of the ZnO thin films*

Figure 6 presents the variation of the samples resistivity as a function of the Aluminum dopant concentration. The electrical resistivity was measured by a four-point probe method.

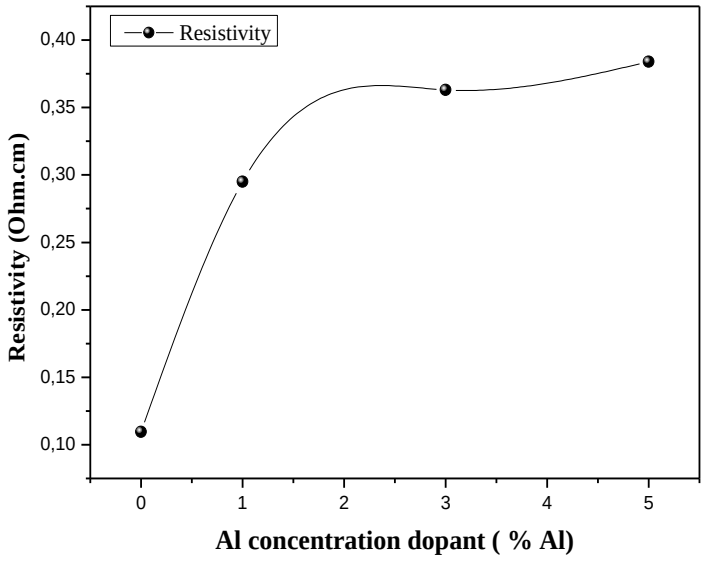

Figure 6: Variation of the resistivity of ZnO:Al films as a function of aluminum concentration.

A minimum resistivity is obtained for undoped ZnO thin films. While increasing the Aluminum concentration from 1% to 5%, the resistivity slightly increases from 2,95 $.10^{-1}$ Ω.cm to 3,84 $.10^{-1}$ Ω.cm.

It is strange that the aluminum atoms don't act as donors and therefore not improve the electrical conductivity of our films. This is probably due to the incorporation of aluminum in the inappropriate sites inducing an amorphization of the films as observed by M.Yilmaz et al. [16] R. H Kimet al [31].

There are two types of interactions:

- Interactions between the charge carriers and the grain boundaries.
- And interactions between charge carriers electron-electron which reduce the mobility.

In our case the mobility of free electrons in the films was improved while increasing the doping, this is due to a reduction of collisions between the charge carriers following a reduction in their density. Which suggests that the interaction between the charge carriers and the grain boundaries that increases in size for our case, was the dominance responsable for the decrease in films conductivity.

Figure 7 presents the variation of the carriers density and mobility as a function of the Aluminum dopant concentration. The carriers density and mobility are performed by Hall effect measurements, and exhibit with increasing the doping Aluminum content, a decrease in the carriers density in the same time an increase in mobility. This decrease in the density of charge carriers is due to an incorporation of aluminum atoms in the interstitial sites of the crystal, also the presence of grain boundaries has played a major role in trapping the charge carriers and subsequently decrease their number. For cons, the mobility of free electrons in the films has improved while increasing the doping, this is probably due to a reduction of collisions between the charge carriers following a reduction in their number as reported by F. Z Ghomrani et al [26] and Ü Özgür et al [27].

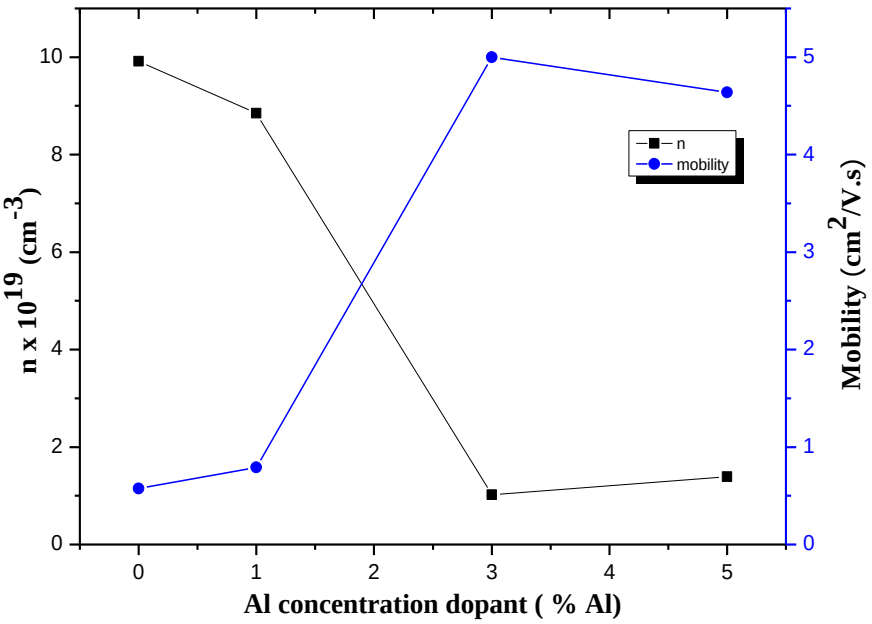

Figure 7: Variation of the mobility and carriers density of ZnO:Al films as a function of aluminum concentration.

Conclusions

The aim of our work was the study of Al-doping concentration on the characteristics of undoped and aluminum doped ZnO films deposited using spin coating method. In this work, we have noted a bad insertion of Aluminum doping in our films, inducing degradation of their structural, optical and electrical properties. Our future investigations will be the study of the effect of other precursors to obtain ZnO thin films perfectly transparent and less resistive, necessary for photo-voltaic modules.

References

1. Nasr B., Dasgupta S., Wang D., Mechau N., Kruk R., Hahn H., *J. Appl. Phys*. 108 (2010) 103721.
2. Beyer W., Hupkes J., Stiebig H., *Thin Solid Films.* 516 (2007) 147.

3. Zargou S., Chabane Sari S.M., Senoudi A.R., Aida M., Attaf N., Hakem I.F., *J. Mater. Environ. Sci*. 7 (2016) 3134.
4. Shrisha B.V., Bhat S., Kushavahb D., Naik K.G., *Mater. Today. Proc*. 3 (2016) 1693.
5. Chen Y., Bagnall D.M., Koh H.J., Park K.T., Hiraga K., Zhu Z.Q., Yao T., *J. Appl. Phys*. 84 (1998) 3912.
6. Benkara S., Zerkout S., *J. Mater. Environ. Sci*. 1 (2010) 173.
7. Dang W.L., Fu Y.Q., Luo J.K., Flewitt A.J., Milne W.I., *Superlattices Microstruct.* 42 (2007) 89.
8. Chang P.C., Zhiyong F., Wang D., Tseng W.Y., Chiou W.A., Hong J., Lu J.G., *Chem. Mater*. 16 (2004) 5133.
9. Harati M., Love D., Lau W. M., Ding Z., *Mater. Lett*.. 89 (2012) 339.
10. Aranovich J., Ortiz A., Bube R.H., *J. Vac. Sci. Technol*. 16 (1979) 994.
11. Gahtar A., Rahal A., Benhaoua B., Benramache S., *Optik.* 125 (2014) 3674.
12. Tomakin M., *Superlattices Microstruct*. 51 (2012) 372.
13. Kim Y.S., Tai W.P., *Appl. Surf. Sci*. 253 (2007) 11.
14. Hussein H.F., Shabeeb G.M., Hashim S.Sh., *J. Mater. Environ. Sci*. 2 (2011) 423.
15. Djouadi D., Chelouche A., Aksas A., *J. Mater. Environ. Sci*. 3 (2012) 585.
16. Yilmaz M., Tatar D., Sonmez E., Cirak C., Aydogan S., Gunturkun R., *Synth. React. Inorg. Met.-Org. Chem.* 46 (2015) 489.
17. Ilican S., Caglar Y., Caglar M., Demirci B., *J. optoelectr. Advanc. mater.* 10 (2008) 2592.
18. Tsay C.Y., Fan K.S., Lei C.M., *J. Alloys. Compd.* 512 (2012) 216.
19. Xu Z.Q., Deng H., Li Y., Guo Q.H., Li Y.R., *Mater. Res. Bull*. 41 (2006) 354.
20. Janotti A., Van de Walle C.G., *Rep. Prog. Phys.* 72 (2009) 29.
21. Coman T., Ursu E.L., Nica V., Tiron V., Olaru M., Cotofana C., Dobromir M., Coroaba A., Dragos O.G., Lupu N., Caltun O.F., Ursu C., *Thin Solid Films*. 571 (2014) 198.
22. Williamson G.K., Hall W.H., *Acta Metall.* 1 (1953) 22.
23. Shrestha S.P., Rishi G., Nakarmi J.J., Kim Y.S., Shrestha S., Park C.Y., Jin-Hyo B., *Bull. Korean Chem*. 31 (2010) 112.
24. Chouikh F., Beggah Y., Aida M.S., *Int. J. Thin Fil. Sci. Tec*. 3 (2014) 51.
25. Tauc J., Menthe A., *J. Non-Cryst. Sol*. 569 (1972) 8.
26. Burstein E., *Phys. Rev*. 93 (1954) 632.
27. Moss T.S., *Proc. Phys. Soc. Lond*. B. 67 (1954) 775.
28. Mridha S., Basak D., *J. Phys. D: Appl. Phys*. 40 (2007) 6902.
29. Urbach F., *Phys. Rev*. 92 (1953) 1324.
30. Pawar B.N., Jadkar S.R., Takwal M.G., *Sol. Energy Mater. Sol. Cells*. 93 (2009) 1417.
31. Kim R.H., Jin B.S., Wen L., Choi S.Y., Choi S.I., Hori M., Han G.J., *J. Ceram. Proces. Res*. 14 (2013) 188.
32. Ghomrani F.Z., Aissat A., Arbouz H., Benkouider A., *Energy Procedia*. 74 (2015) 491.
33. Özgür Ü., Alivov Ya.I., Liu C., Teke A., Reshchikov M.A., *J. Appl. Phys*. 98 (2005) 041301.